Journal of Power Sources 195 (2010) 3742–3747

Contents lists available at ScienceDirect

Journal of Power Sources

journal homepage: www.elsevier.com/locate/jpowsour

Synthesis and pseudocapacitive studies of composite films of polyaniline and manganese oxide nanoparticles

Liang Chen[a], Li-Jie Sun[a], Feng Luan[a], Ying Liang[a], Yat Li[b,*], Xiao-Xia Liu[a,**]

[a] Department of Chemistry, Northeastern University, Shenyang 110004, China
[b] Department of Chemistry and Biochemistry, University of California, 1156 High Street, Santa Cruz, CA 95064, USA

ARTICLE INFO

Article history:
Received 19 November 2009
Received in revised form 7 December 2009
Accepted 8 December 2009
Available online 16 December 2009

Keywords:
Polyaniline
Manganese oxide nanoparticles
Molecular linker
Pseudocapacitive studies

ABSTRACT

We report the synthesis and pseudocapacitive studies of a composite film (PANI-ND-MnO_2) of polyaniline (PANI) and manganese oxide (MnO_2) nanoparticles. To enhance the interaction of MnO_2 and PANI, the surfaces of MnO_2 nanoparticles were modified by a silane coupling reagent, triethoxysilylmethyl N-substituted aniline (ND42). The composite film was obtained via controlled electro-co-polymerization of aniline and N-substituted aniline grafted on surfaces of MnO_2 nanoparticles (ND-MnO_2) on a carbon cloth in a electrolyte of 0.5 M H_2SO_4 and 0.6 M $(NaPO_3)_6$. In comparison to similarly prepared PANI film, the incorporation of MnO_2 nanoparticles substantially increases the effective surface area of the film by reducing the size of rod-like PANI aggregates and avoiding the entanglement of these PANI nanorods. Significantly, we observed significant enhancement of specific capacitance in PANI-ND-MnO_2 film compared to PANI–MnO_2 film prepared in a similar condition, indicating that the presence of the coupling reagent can improve the electrochemical performance of PANI composite film. A symmetric model capacitor has been fabricated by using two PANI-ND-MnO_2 nanocomposite films as electrodes. The PANI-ND-MnO_2 capacitor showed an average specific capacitance of ~80 F g^{-1} and a stable coulombic efficiency of ~98% over 1000 cycles. The results demonstrated that PANI-ND-MnO_2 nanocomposites are promising materials for supercapacitor electrode and the importance of designing and manipulating the interaction between PANI and MnO_2 for fundamentally improving capacitive properties.

1. Introduction

Electrochemical capacitors, known as supercapacitors (SCs), are charge-storage devices that capable of very fast charges and discharges, with a unique combination of high power, high energy and long lifetime [1]. SCs with these unique properties can bridge the gap between batteries and capacitors, offering great potentials in applications such as starting automotives and regenerating of brake energy. To date, carbon [2–5], transition metal oxides [6–10] and conducting polymers [11,12] have been identified as most promising materials for SCs. Each material has its own unique advantages and disadvantages for SC applications. For example, carbon SCs have been widely investigated and used in the recent years due to its high power density and long life cycle [1–4]. However, the small double layer capacitance of carbon limits its application for high energy density devices [1,13]. Transition metal oxides such as hydrous RuO_2 [14], NiO [15,16], CoO_x, and MnO_2 [17] have been studied and implemented as electrode materials for SCs [1,6–10]. Although they have wide charge/discharge potential range, most of the transition metal oxides have relatively low capacitance [6,9]. Conducting polymers such as polyaniline (PANI) have been considered as another promising material in the redox SCs. Although they have advantages such as high capacitance, high conductivity, low cost and ease of fabrication [11], the relatively low mechanical stability and cycle life are major limitations for applications.

In recent years, considerable efforts have been placed to couple the unique advantages of these capacitive materials for SCs [18–23]. The synthesis and studies of composites of PANI and MnO_2 have attracted much attention due to the low cost and environment friendliness of the active materials. The PANI–MnO_2 composite films have been synthesized using different chemical methods [19,24–29]. The PANI not only serves as an electroactive material for energy storage but also a good coating layer to restrain MnO_2 from dissolution in acidic electrolytes [24]. It has been reported that the composite obtained through intercalation of PANI into layers of MnO_2 showed an enhanced specific capacitance of 330 F g^{-1} due to the synergistic effects [25]. In comparison to chemical methods, electrochemical deposition offer better control of the thickness of the composite film and ease in constructing modified

* Corresponding author. Tel.: +1 831 459 1952; fax: +1 831 459 2935.
** Corresponding author. Tel.: +86 24 83689510; fax: +86 24 23600159.
E-mail addresses: yli@chemistry.ucsc.edu (Y. Li), xxliu@mail.neu.edu.cn (X.-X. Liu).

0378-7753/$ – see front matter © 2009 Elsevier B.V. All rights reserved.
doi:10.1016/j.jpowsour.2009.12.036

electrodes [17,26–29]. For example, Prasad reported the electrodeposition of PANI–MnO_2 composites, which showed high specific capacitance of 715 F g^{-1} and excellent cyclic performance [29]. Liu reported the electrochemical-doping-deposition method, where the MnO_2 nanoparticles can be distributed in three-dimensional matrix of PANI doped polymers [27,28]. We have recently demonstrated the preparation of composite films of PANI and MnO_x by electro-co-deposition method using aniline and $MnSO_4$ as precursors [17,26]. The in situ incorporation of active materials in co-deposition method could dramatically affect the polymerization process of aniline and thereby the surface morphologies of obtained PANI and MnO_2 composites. However, our previous work [26] showed that the relatively weak interaction between PANI and transition metal oxides limits the capacitive properties of the composite films. Here we report a new synthetic strategy for inclusion of MnO_2 nanoparticles into a film of PANI through electro-co-polymerization of aniline and N-substituted aniline grafted on surfaces of MnO_2 nanoparticles, using the silane coupling agent, triethoxysilylmethyl N-substituted aniline (ND42) as linker molecule. Significantly, the presence of surface modified MnO_2 nanoparticles increases active surface area of the PANI and MnO_2 composite film and thereby enhances the electrochemical performance.

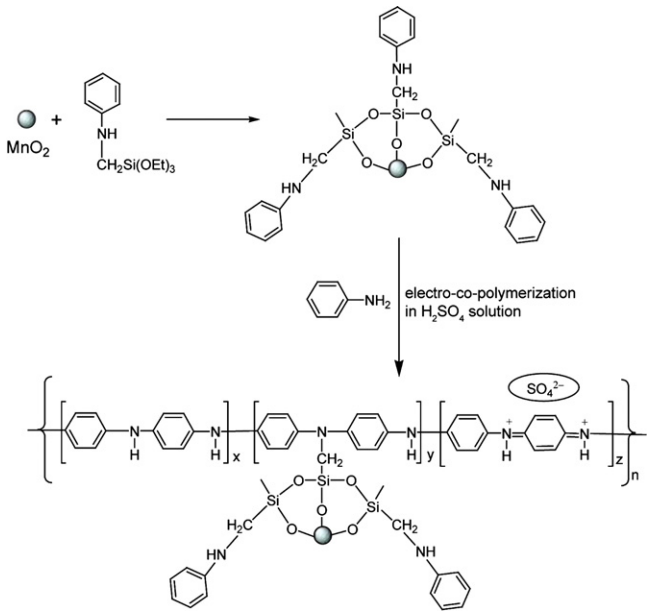

Fig. 1. A schematic diagram illustrates the reaction pathway for the synthesis of PANI-ND-MnO_2 nanocomposite film.

2. Experimental

2.1. Materials and instrumentation

All reagents except aniline were analytically pure and used as received. Aniline was distilled under reduced pressure before use. Carbon cloth was purchased from SGL Group (Germany). X-ray diffraction (XRD) patterns of MnO_2 nanoparticles were recorded on a PANalytical PW3040/60 X-ray diffractometer. The scanning electron microscopy (SEM) images of the nanocomposite films were collected in a SHIMADZU SSX 550 SEM. MnO_2 nanoparticles were dispersed in ethanol solution and then transferred onto Cu/laceycarbon transmission electron microscopy (TEM) grids. TEM images were collected in a FEI TECNAI G2 TEM system operated with a 200 kV electron beam. Fourier Transform Infrared (FT-IR) spectra were collected from KBr pellets made of the nanocomposite materials using a Spectrum One FT-IR spectrophotometer. Electrochemical experiments were conducted on a Shanghai Chenhua CHI 760 C electrochemical analyzer.

2.2. Preparation and surface modification of MnO_2 nanoparticles (ND-MnO_2)

Surface modified MnO_2 nanoparticles were prepared in two steps. First, MnO_2 nanoparticles were synthesized using modified hydrothermal method reported previously [30]. A mixture of $MnSO_4$ (1.0 M) and $KMnO_4$ (0.5 M) solution was stirred for 4 h at 70 °C. The obtained precipitates were washed several times with distilled water followed by ethanol to remove impurities, and then dried in vacuum at 110 °C for 5 h. The dried powder was put into muffle and heated at 300 °C for additional 3 h. These powders were acidified with 2.0 M H_2SO_4 at 90 °C for 2 h. Finally, the product was washed with distilled water and vacuum dried.

Second, MnO_2 nanoparticles were modified with silane coupling agent, ND42, as illustrated in Fig. 1. 0.2 g MnO_2 nanoparticles were treated in 80 ml boiling water for 1 h to increase percentage of –OH coverage on surfaces of the nanoparticles. The hydroxylated nanoparticles were dispersed in 50 ml mixture of water and ethanol (30:70, v:v), together with 0.2 ml ND42 pre-hydrated in small amount of water. The solution mixture was sonicated at 65 °C for 30 min and stirred at 80 °C for additional 4 h. The obtained surface modified MnO_2 nanoparticles (ND-MnO_2) were washed thoroughly with ethanol followed by water, and then dried at 50 °C for 6 h.

2.3. Electrochemical synthesis and studies of PANI-ND-MnO_2 nanocomposite film

All electrochemical experiments were performed in an electrochemical cell using saturated calomel electrode (SCE) as reference and platinum wire as counter electrode. Electro-co-polymerization of aniline and ND-MnO_2 nanoparticles was conducted on a carbon cloth in an electrolyte solution containing 0.2 g L^{-1} ND-MnO_2 and 0.1 M aniline, 0.5 M H_2SO_4 and 0.6 g L^{-1} $(NaPO_3)_6$ (Fig. 1). The co-polymerization was preceded through 50 successive cyclic voltammetric scans from −0.21 to 0.91 V at a scan rate of 10 mV s^{-1}. PANI–MnO_2 films (without ND42 linker) and PANI films were prepared as control samples in similar conditions. The loading of the films was measured by the weight difference of the electrode (vacuum dried at room temperature) before and after electrodeposition, using Sartorius BT 25 S microbalance with an accuracy of 0.01 mg.

Electroactivities of the films were studied through cyclic voltammetric scans at a rate of 5 mV s^{-1} in a 0.5 M H_2SO_4 electrolyte. Pseudocapacitive properties of the films were studied through constant current charging–discharging experiments by chronopotentiometry (CP) at 1.67 mA cm^{-2} (the geometric area of the electrode is 0.6 cm^2). The electrolyte was 1.0 M $NaNO_3$ and the pH of the solution was adjusted to be 1 by adding HNO_3. A symmetric model capacitor was constructed using two PANI-ND-MnO_2 films as electrodes. The pseudocapacitive properties of the cells were investigated by CV and CP in 1.0 M $NaNO_3$ electrolyte.

3. Results and discussion

3.1. Material characterization

To monitor the reaction and understand the structural properties of the product in each reaction step, we carried out systematic material characterization using a combination of electron microscopy and spectroscopy techniques. As shown in Fig. 2a, TEM image reveal that MnO_2 nanoparticles are uniform in diameter (∼15–20 nm) with typical lengths of ∼10–80 nm. Fig. 2b shows the

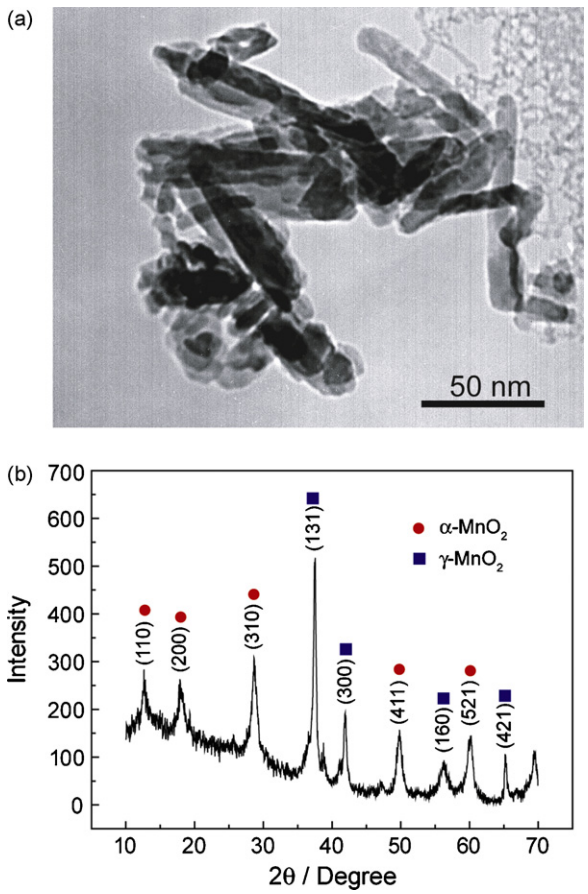

Fig. 2. (a) Bright-field TEM image and (b) XRD spectrum collected from as prepared MnO_2 nanoparticles.

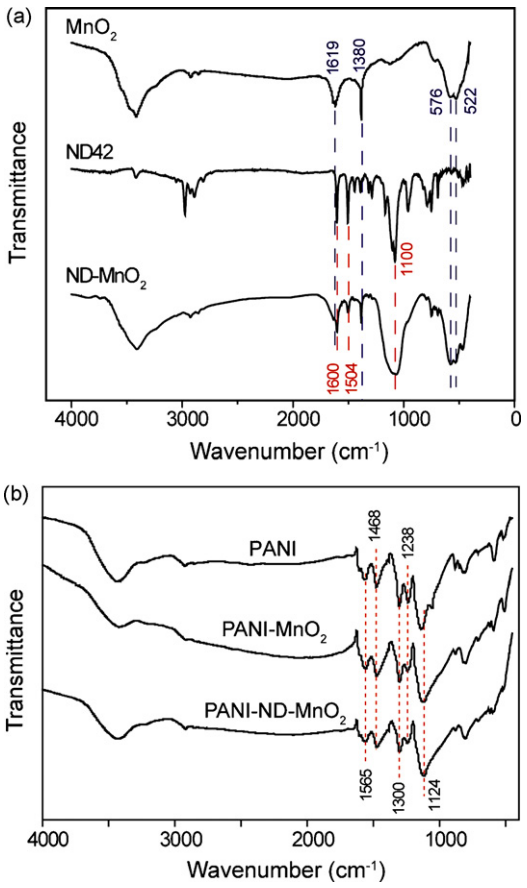

Fig. 3. (a) FT-IR spectra of MnO_2, ND42 and ND-MnO_2 and (b) FT-IR spectra of PANI, PANI–MnO_2 and PANI-ND-MnO_2 films.

XRD pattern of the MnO_2 nanoparticles. The XRD spectrum consists of two sets of diffraction pattern, which can be indexed to tetragonal α-MnO_2 (red circle, JCPDS No. 44-0141) and orthorhombic γ-MnO_2 (blue square, JCPDS No. 14-0644) crystal structures, respectively. These XRD result indicates the as prepared MnO_2 nanoparticles are crystalline material, with α- and γ-phase structure co-existed in the product.

We modified the surface of these MnO_2 nanoparticles with silane-containing agent, ND42. FT-IR measurements were conducted to monitor and verify the chemical anchoring of the ND42 onto MnO_2 surface. Fig. 3a compares the FT-IR absorption spectra collected from MnO_2, ND42 and ND-MnO_2. The FT-IR spectrum of MnO_2 shows characteristic Mn–O vibrational peaks centered at 522 and 576 cm^{-1}, while other two pronounced peaks centered at 1387 and 1619 cm^{-1} are O–H stretching vibrations on Mn atom, as reported previously [18,31]. The dominant vibrational peaks observed in the spectrum of ND42 can be attributed to the stretching peaks of carbon skeleton of phenyl ring (1504 and 1600 cm^{-1}) and anti-symmetric stretching peak of Si–O (1100 cm^{-1}), respectively [32]. Significantly, we observed all the characteristic IR peaks of MnO_2 and ND42 in ND-MnO_2 sample, confirming that the surface of MnO_2 had been modified by ND42.

MnO_2 nanoparticle loaded polyaniline (PANI–MnO_2 and PANI-ND-MnO_2) films were prepared by electropolymerization of aniline in the presence of MnO_2 and ND-MnO_2 nanoparticles, respectively, through successive cyclic voltammetric scans. As shown in Fig. 3b, the FT-IR spectra obtained from both PANI–MnO_2 and PANI-ND-MnO_2 composite samples showed characteristic peaks of PANI. For example, vibrational peaks centered at 1565 and 1468 cm^{-1} are attributed to the stretching peaks of quinoid and benzenoid deformations of PANI (Fig. 3b) [33]. We also observed C–N stretching peaks of 1238 and 1300 cm^{-1} and C–H bending of protonated PANI at 1124 cm^{-1}. The characteristic IR peaks of MnO_2 were not observed due to the low loading of MnO_2 nanoparticles, the results suggest that the PANI–MnO_2 and PANI-ND-MnO_2 composites are mainly compose of PANI.

The chemical composition and structural properties of the composite films were examined by SEM. As shown in Fig. 4, we observed Mn signals in the energy dispersive X-ray spectroscopy

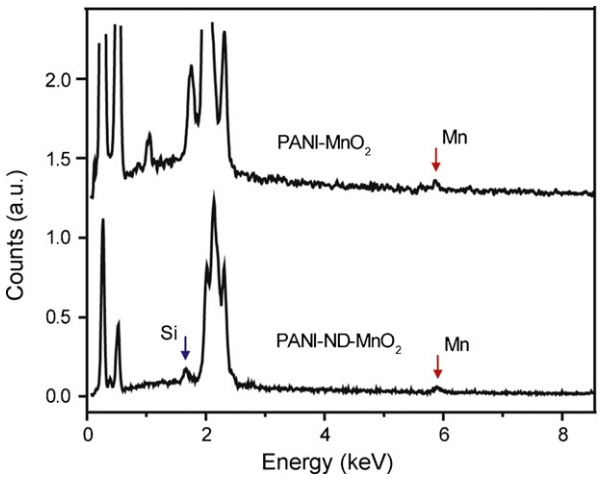

Fig. 4. EDS spectra of PANI–MnO_2 and PANI-ND-MnO_2 composite films. Arrows highlighted the Mn (red) and Si (blue) peaks. (For interpretation of the references to color in this figure legend, the reader is referred to the web version of the article.)

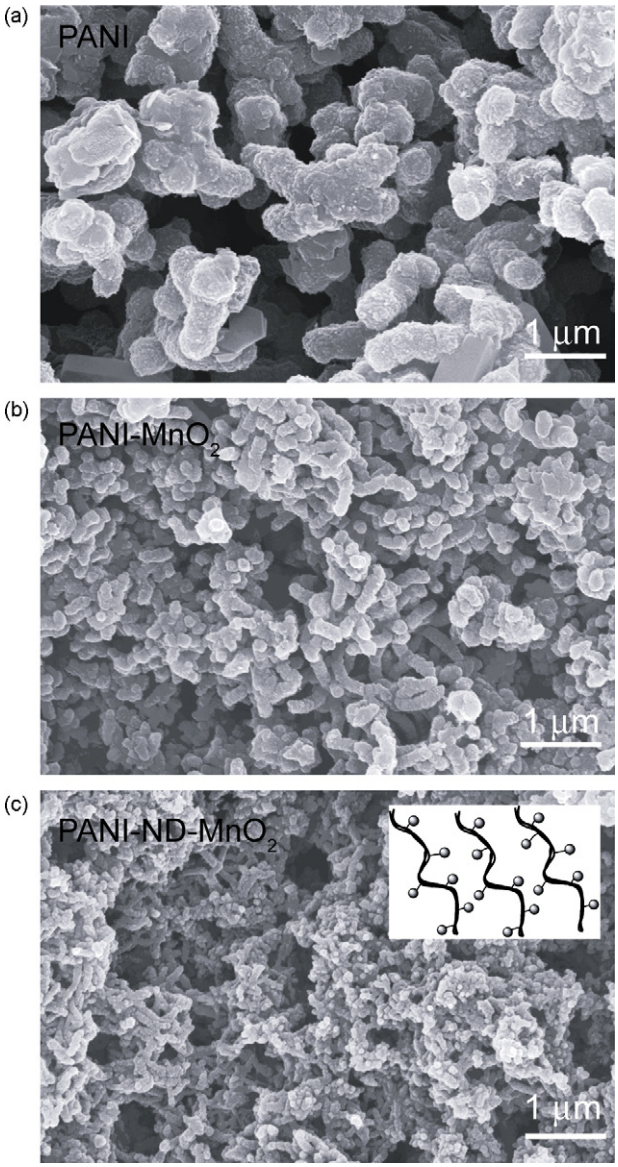

Fig. 5. SEM images of (a) PANI polymer film, (b) PANI–MnO_2 composite film, and (c) PANI-ND-MnO_2 composite film. Inset: a scheme showing ND-MnO_2 nanoparticles anchor on PANI chains.

data collected from PANI–MnO_2 and PANI-ND-MnO_2 films, confirming the successful integration of MnO_2 nanoparticles to PANI in the composite structures. SEM images showed that the blank PANI film is constructed with rod-like aggregates that typically are ~400–500 nm in diameter and ~1 μm in length (Fig. 5a). PANI chains are prepared in acidic media and exist in the form of polycations. The strong electrostatic interactions between charged PANI chains [34] facilitate the formation of 1D nanorods or nanofibers without the need of structure directing agent or template [35]. The formation of rod-like aggregates can be attributed to the secondary growth of the 1D PANI structures during the early stage of polymerization [36].

The SEM images of PANI–MnO_2, PANI-ND-MnO_2 films reveal that the addition of MnO_2 nanoparticles promotes the one-dimensional (1D) growth of PANI, which substantially reduces the size of the nanorods and increases the surface area/internal space of the composite films (Fig. 5). The typical sizes of PANI rods in three films are, PANI: diameter ~500 nm, length ~1 μm; PANI–MnO_2: diameter ~200 nm, length ~700 nm; PANI-ND-MnO_2: diameter ~150 nm, length ~400 nm. Since the densities of the three composite films are similar, the surface to volume ratio is a good indication of the active surface area of these films. The surface area to volume ratio of a single PANI rod in these three composite films are about 0.018 nm^{-1} (PANI-ND-MnO_2); 0.013 nm^{-1} (PANI–MnO_2); and 0.01 nm^{-1} (PANI), respectively, indicates the PANI-ND-MnO_2 film has substantially enhanced surface area. Great efforts have been placed to reduce the secondary growth of PANI in order to get fibrous structures [35,37]. Kan and coworkers reported the construction of PANI nanofibers was facilitated by intermolecular H-bonding between methanol and PANI, which pushed the polymer chains apart [38]. Similarly, the H-bonding interaction between PANI and MnO_2 nanoparticles during co-polymerization process could inhibit the secondary growth perpendicular to PANI chains and direct the 1D growth of the polymer. In addition, the incorporation of MnO_2 nanoparticles would effectively avoid the entanglement of PANI chains due to the electrostatic repulsion between positive charged MnO_2 nanoparticles in an acidic co-polymerization media (Fig. 5c, inset). In comparison to PANI–MnO_2 film, PANI-ND-MnO_2 film consists of smaller size PANI nanorods with higher surface area, indicating a stronger interaction between MnO_2 and PANI through ND42 linker molecule. The increase of active surface area of the composite films could lead to a significant enhancement of Faraday pseudocapacitance.

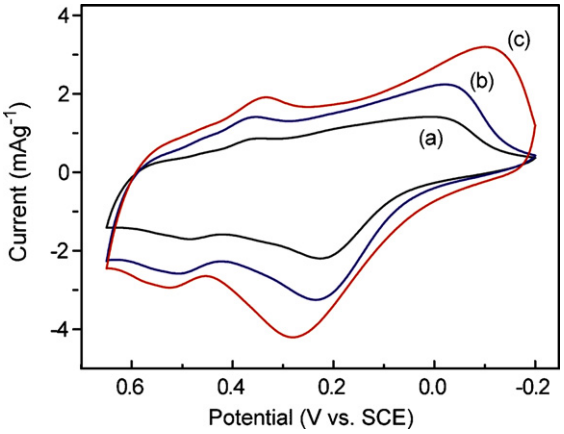

Fig. 6. Cyclic voltammograms collected from (a) PANI, (b) PANI–MnO_2 and (c) PANI-ND-MnO_2 film in 0.5 M H_2SO_4 at a scan rate of 5 mV s^{-1} vs. SCE.

3.2. Electrochemical studies of PANI composite films

CV measurements were performed to investigate the influence of MnO_2 nanoparticles on the electrochemical properties of PANI film. Fig. 6 shows the CV spectra of PANI film, PANI–MnO_2 and PANI-ND-MnO_2 composite films collected in the potential range of −0.20 to +0.65 V at a scan rate of 5 mV s^{-1} using 0.5 M H_2SO_4 as electrolyte. We observed the characteristic redox exchange between emeraldine and leucoemeraldine states of PANI in all samples [39]. The PANI-ND-MnO_2 composite film showed the highest current densities among the samples, which is in agreement with the highest effective surface area of PANI-ND-MnO_2 film.

To investigate capacitive properties, the galvanostatic charge–discharge measurements were carried out on these films in a 1.0 M $NaNO_3$ electrolyte at different discharge currents of 1.00, 2.36, 3.00, 5.00, 7.10 mA. Representative charge–discharge curves recorded at 1.00 mA are depicted in Fig. 7. The constant slope of these discharge curves reveals that the films have excellent electrochemical reversibility and capacitive characteristics, which are critical for SC applications. Significantly, we observed the IR drop decreases from 60 mV for PANI to 40 mV for PANI–MnO_2 and 30 mV for PANI-ND-MnO_2. The IR drop is attributed to the

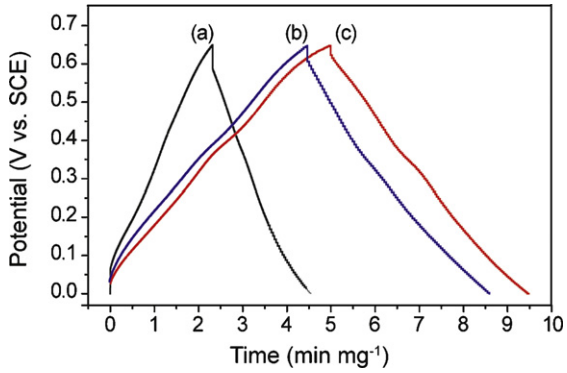

Fig. 7. CP spectra of (a) PANI, (b) PANI–MnO_2 and (c) PANI-ND-MnO_2 in 1.0 M $NaNO_3$ (adjusted to pH 1) at 1.67 mA cm^{-2}.

equivalent series resistance which arises from the resistance of both the electrolyte and the electrode [11]. These results indicate that the conductivities of the composite films are improved upon the inclusion of MnO_2 nanoparticles.

The average specific capacitance (C) of these films can be calculated from Eq. (1) [4]:

$$C = \frac{i \cdot t}{\Delta E \cdot W} \quad (1)$$

where i is the discharging current, t the time, ΔE the discharging potential window and W is the amount of the active material on the electrodes. The calculated specific capacitances of these films were plotted as a function of discharge current density (Fig. 8). The films exhibit similar charge–discharge behaviors, where the specific capacitance decreases as the discharge current increase. In comparison to PANI film, the composite films with MnO_2 nanoparticles exhibit about two times enhanced specific capacitance due to the higher effective surface area of PANI and the capacitance contributed from the incorporated MnO_2 nanoparticles. Significantly, the PANI-ND-MnO_2 film showed additional ~10% enhancement in specific capacitance compared to PANI–MnO_2 film, which is in agreement with the improved surface area of PANI-ND-MnO_2 film by adding the linker molecule ND42. The maximum specific capacitance of the PANI-ND-MnO_2 composite film is 415 F g^{-1} at a discharge current density of 1.67 mA cm^{-2}.

A symmetric model capacitor was fabricated by using two PANI-ND-MnO_2 composite films as electrodes. Cyclic voltammograms of these capacitors were measured in 1.0 M $NaNO_3$ electrolyte, with scan rates at 1, 2, 5, 10, 25 mV s^{-1}, as shown in Fig. 9. We observed two important features from the cyclic voltammograms. First, the absence of redox peaks indicates that the SC is charged and discharged at a pseudo-constant rate over the whole voltammetric

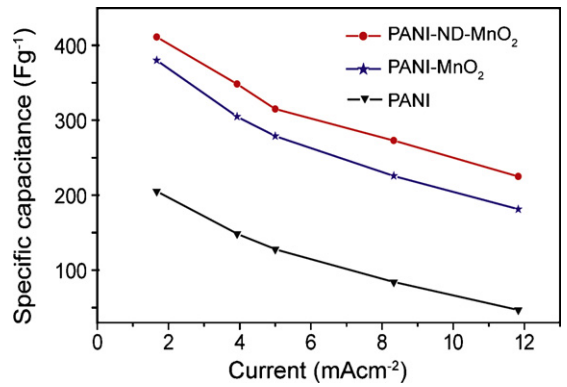

Fig. 8. The specific capacitance collected from PANI, PANI–MnO_2 and PANI-ND42-MnO_2 films as a function of discharge current density in a 1.0 M $NaNO_3$ electrolyte.

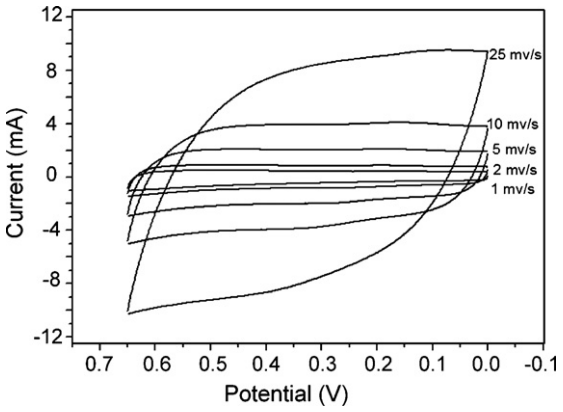

Fig. 9. Cyclic voltammograms of the capacitor fabricated from PANI-ND-MnO_2 films measured at scan rates of 1, 2, 5, 10, 25 mV s^{-1}.

cycle. Second, we observed a square voltammetric response with marginal IR effects at low scan rates up to 10 mV s^{-1}, indicating that the composite film exhibit high intrinsic electrical conductivity as well as good kinetic reversibility, which are important factors for capacitor behavior. As the scan rate increases, however, the deviation from rectangularity of the CV becomes obvious. The distorted current response at the switching potential can be attributed to the electrolyte and film resistance, and this distortion is depending on scan rate.

To evaluate the performance of these PANI-ND-MnO_2 films for SCs, the specific capacitance of the PANI-ND-MnO_2 capacitor was measured in a constant charging–discharging experiment at a discharge current of 2.36 mA over 1000 cycles (Fig. 10). According to Eq. (1), the average specific capacitance of the PANI-ND-MnO_2 capacitor is calculated to be 87 F g^{-1}, around one fourth of that of one film electrode, as expected. It is because the mass of active material is doubled and two electrodes are connected in series. The capacitor showed a slight decrease of specific capacitance in the first 200 cycles and then become stable at ~75 F g^{-1}. Significantly, the capacitor shows a reduction of less than 15% of the discharge capacity after 1000 cycles, indicating the excellent stability of this nanocomposite material for energy storage applications. In addition, the coulombic efficiency (η) of the capacitor was calculated base on the following equation

$$\eta = \left(\frac{t_D}{t_C}\right) \times 100 \quad (2)$$

where t_D and t_C are discharging and charging times, respectively. These results reveal that the capacitor has a very stable coulombic efficiency of ~98% over 1000 cycles (Fig. 10).

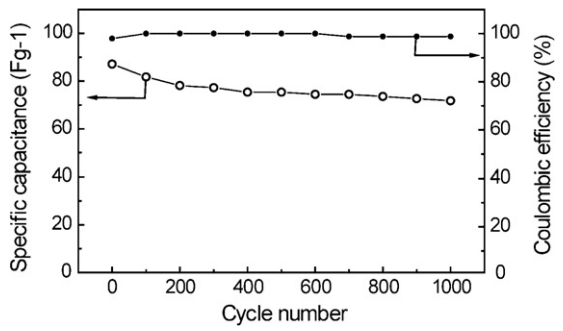

Fig. 10. The specific capacitance and coulombic efficiency of a symmetric capacitor made of two PANI-ND-MnO_2 films as electrodes, measured in charging–discharging cycles at a constant current of 2.36 mA.

4. Conclusions

In summary, we have synthesized a nanocomposite film based on polyaniline nanorods and MnO_2 nanoparticles with properties tailored for supercapacitors. We observed an enhanced specific capacitance in PANI-ND-MnO_2 film compared to the PANI–MnO_2 film prepared in a similar condition. The enhancement can be attributed to the improved interaction between MnO_2 and PANI and the increased effective surface area in PANI-ND-MnO_2 film, due to the surface modification of MnO_2 nanoparticles with the silane coupling reagent. Cyclic voltammograms showed that the PANI-ND-MnO_2 composite film exhibit high intrinsic electrical conductivity and good kinetic reversibility. In addition, the constant charging–discharging experiments reveal that the PANI-ND-MnO_2 capacitor has an average specific capacitance of $\sim 80\,F\,g^{-1}$ and a very stable coulombic efficiency of ~98% over 1000 cycles. This work demonstrated a simple way to enhance the interaction of PANI and MnO_2 in a composite film, and provides useful insights for developing new nanocomposite structures for supercapacitors.

Acknowledgements

X.X.L. gratefully acknowledges financial support from National Natural Science Foundation of China (project number: 50973013) and Natural Science Foundation of Liaoning Province, China (project number: 20052016). Y.L. thanks the support of this work by UCSC new faculty startup fund.

References

[1] P. Simon, Y. Gogotsi, Nat. Mater. 7 (2008) 845–854.
[2] A.B. Fuertes, F. Pico, J.M. Rojo, J. Power Sources 133 (2004) 329–336.
[3] J. Gamby, P.L. Taberna, P. Simon, J.F. Fauvarque, M. Chesneau, J. Power Sources 101 (2001) 109–116.
[4] D. Qu, H. Shi, J. Power Sources 74 (1998) 99–107.
[5] M. Kaempgen, C.K. Chan, J. Ma, Y. Cui, G. Gruner, Nano Lett. 9 (5) (2009) 1872–1876.
[6] E. Beaudrouet, A. Le Gal La Salle, D. Guyomard, Electrochim. Acta 54 (2009) 1240–1248.
[7] Y.G. Wang, Y.Y. Xia, Electrochim. Acta 51 (2006) 3223–3227.
[8] T.Y. Wei, C.H. Chen, K.H. Chang, S.Y. Lu, C.C. Hu, Chem. Mater. 21 (2009) 3228–3233.
[9] P. Yu, X. Zhang, D. Wang, L. Wang, Y. Ma, Cryst. Growth Des. 9 (2009) 528–533.
[10] J.P. Zheng, T.R. Jow, J. Power Sources 62 (1996) 155–159.
[11] H. Li, J. Wang, Q. Chu, Z. Wang, F. Zhang, S. Wang, J. Power Sources 190 (2009) 578–586.
[12] W. Sun, X. Chen, J. Power Sources 193 (2009) 924–929.
[13] A. Lewandowski, M. Galinski, J. Power Sources 173 (2007) 822–828.
[14] C.C. Hu, K.H. Chang, M.C. Lin, Y.T. Wu, Nano Lett. 6 (12) (2006) 2690–2695.
[15] C. Yuan, X. Zhang, L. Su, B. Gao, L. Shen, J. Mater. Chem. 19 (2009) 5772–5777.
[16] K.C. Liu, M.A. Anderson, J. Electrochem. Soc. 143 (1) (1996) 124–130.
[17] L.J. Sun, X.X. Liu, K.K.T. Lau, L. Chen, W.M. Gu, Electrochim. Acta 53 (2008) 3036–3042.
[18] A. Yuan, Q. Zhang, Electrochem. Commun. 8 (2006) 1173–1178.
[19] C. Bian, A. Yu, H. Wu, Electrochem. Commun. 11 (2009) 266–269.
[20] J.H. Kim, A.K. Sharma, Y.S. Lee, Mater. Lett. 60 (2006) 1697–1701.
[21] J. Yan, Z. Fan, T. Wei, J. Cheng, B. Shao, K. Wang, L. Song, M. Zhang, J. Power Sources 194 (2009) 1202–1207.
[22] P. Barpanda, Y. Li, F. Cosandey, S. Rangan, R.A. Bartynski, G.G. Amatucci, J. Electrochem. Soc. 156 (11) (2009) A873–A885.
[23] L.Z. Fan, Y.S. Hu, J. Maier, P. Adelhelm, B. Smarsly, Antonietti, Adv. Funct. Mater. 17 (2007) 3083–3087.
[24] C. Yuan, L. Su, B. Gao, X. Zhang, Electrochim. Acta 53 (2008) 7039–7047.
[25] X. Zhang, L. Ji, S. Zhang, W. Yang, J. Power Sources 173 (2007) 1017–1023.
[26] L.J. Sun, X.X. Liu, Eur. Polym. J. 44 (2008) 219–224.
[27] F.J. Liu, T.F. Hsua, C.H. Yang, J. Power Sources 191 (2009) 678–683.
[28] F.J. Liu, J. Power Sources 182 (2008) 383–388.
[29] K.R. Prasad, N. Miura, Electrochem. Solid-State Lett. 7 (2004) A425–A428.
[30] Y.L. Feng, M.L. Zhang, Y. Chen, Y. Han, Z.H. Shi, J. Chin. Ceram. Soc. 33 (2005) 318–322.
[31] X.F. Xie, L. Gao, Carbon 45 (2007) 2365–2373.
[32] X.X. Liu, Y.Q. Dou, J. Wu, X.Y. Peng, Electrochim. Acta 53 (2008) 4693–4698.
[33] S.X. Wang, L.X. Sun, Z.C. Tan, F. Xu, Y.S. Li, J. Therm. Anal. Calorim. 89 (2) (2007) 609–612.
[34] L.J. Pan, L. Pu, Y. Shi, T. Sun, R. Zhang, Y.O. Zheng, Adv. Funct. Mater. 16 (2006) 1279–1288.
[35] J.X. Huang, R.B. Kaner, Chem. Commun. (2006) 367–376.
[36] J.X. Huang, R.B. Kaner, Angew. Chem. Int. Ed. 43 (2004) 5817–5821.
[37] X.F. Lu, H. Mao, D.M. Chao, W.J. Zhang, Y. Wei, Macromol. Chem. Phys. 207 (2006) 2142–2152.
[38] S. Zhou, T. Wu, J.Q. Kan, Eur. Polym. J. 43 (2007) 395–402.
[39] X.X. Liu, Y.Q. Dou, J. Wu, X.Y. Peng, Electrochem. Acta 53 (2008) 4693–4698.